

Ultra-Low-Energy Germanium Detector for Neutrino-Nucleus Coherent Scattering and Dark Matter Searches

HENRY T. WONG *

Institute of Physics, Academia Sinica, Taipei 11529, Taiwan.

The status and plans of a research program on the development of ultra-low-energy germanium detectors with sub-keV sensitivities are reported. We survey the scientific goals which include the observation of neutrino-nucleus coherent scattering, the studies of neutrino magnetic moments, as well as the searches of WIMP dark matter. In particular, a threshold of 100-200 eV and a sub-keV background comparable to underground experiments were achieved with prototype detectors. New limits were set for WIMPs with mass between 3–6 GeV. The prospects of the realization of full-scale experiments are discussed.

Keywords: Neutrino Properties, Dark matter, Radiation Detector

PACS Nos.: 14.60.Lm, 95.35.+d, 29.40.-n.

1. Introduction

A research program in low energy neutrino and astroparticle physics is being pursued at the Kuo-Sheng(KS) Reactor Laboratory¹. The KS laboratory is located 28 m from a 2.9 GW reactor core and has an overburden of about 30 meter-water-equivalent. Its facilities were described in Ref. ², where limits on neutrino magnetic moments with a 1.06 kg germanium detector (HPGe) at a hardware threshold of 5 keV were reported. The experimental procedures were well-established and the background were measured. In particular, a background level of ~ 1 event $\text{kg}^{-1}\text{keV}^{-1}\text{day}^{-1}(\text{cpd})$ at 20 keV, comparable to those of underground CDM experiments, was achieved. The HPGe data were also used in the studies of reactor electron neutrinos³ and for reactor axions searches⁴. Data taking and analysis are being conducted on a 200 kg CsI(Tl) scintillating crystal detector array⁵, towards the measurement of neutrino-electron scattering cross-section and therefore the electro-weak angle $\sin^2\theta_W$. The future scientific goals are to develop advanced detectors with kg-size target mass, 100 eV-range threshold and low-background specifications for WIMP dark matter searches⁶ as well as the studies of neutrino-nucleus coherent scattering⁷ and neutrino magnetic moments⁸.

*Contact E-mail: htwang@phys.sinica.edu.tw

2 *Henry T. Wong*

2. Physics Motivations and Goals

Results from recent neutrino experiments provide strong evidence for neutrino oscillations due to finite neutrino masses and mixings⁹. Their physical origin and experimental consequences are not fully understood. Experimental studies on the neutrino properties and interactions can shed light on these fundamental questions and constrain theoretical models, from which unexpected surprises may arise. It is therefore highly motivated to look for and establish alternatives of neutrino sources and detection channels, especially in regions of parameter space which are experimentally unexplored.

One of the frontiers is to open the detector window in the previously unexplored low energy “sub-keV” regime. If experimentally realized, several important subjects in neutrino and astroparticle physics can be pursued. They are discussed in the following sub-sections.

2.1. Neutrino-Nucleus Coherent Scattering

Neutrino coherent scattering with the nucleus¹⁰

$$\nu + N \rightarrow \nu + N \quad (1)$$

is a fundamental neutrino interaction which has never been observed. The Standard Model cross section for this process is given by:

$$\begin{aligned} \left(\frac{d\sigma}{dT}\right)_{\text{SM}}^{\text{coh}} &= \frac{G_{\text{F}}^2}{4\pi} m_{\text{N}} [Z(1 - 4\sin^2\theta_{\text{W}}) - N]^2 \left[1 - \frac{m_{\text{N}} T_{\text{N}}}{2E_{\nu}^2}\right] \\ \sigma_{\text{tot}} &= \frac{G_{\text{F}}^2 E_{\nu}^2}{4\pi} [Z(1 - 4\sin^2\theta_{\text{W}}) - N]^2 \end{aligned} \quad (2)$$

where m_{N} , N and Z are the mass, neutron number and atomic number of the nuclei, respectively, E_{ν} is the incident neutrino energy and T_{N} is the measure-able recoil energy of the nucleus. This formula is applicable at $E_{\nu} < 50$ MeV where the momentum transfer (Q^2) is small such that $Q^2 R^2 < 1$, where R is the nuclear size. Corrections due to nuclear form factors can be neglected at low energies: $Q^2 \ll m_{\text{N}}^2$. The $\sim N^2$ enhancement on the cross-sections signifies coherence.

Measurement of the coherent scattering cross-section would provide a sensitive test to the Standard Model^{11,12} probing the weak nuclear charge and radiative corrections due to possible non-standard neutrino interactions or additional neutral gauge bosons. The coherent interaction plays important role in astrophysical processes where the neutrino-electron scatterings are suppressed due to Fermi gas degeneracy. It is significant to the neutrino dynamics and energy transport in supernovae and neutrons stars¹³. Being a new detection channel for neutrinos, it may provide new approaches to study other aspects of neutrino physics. For instance, the detection of supernova neutrinos using this mode was recently discussed¹⁴. Coherent scattering with the nuclei is also the detection mechanism adopted in the direct Dark Matter searches^{9,15}, such that its observations and measurements with the

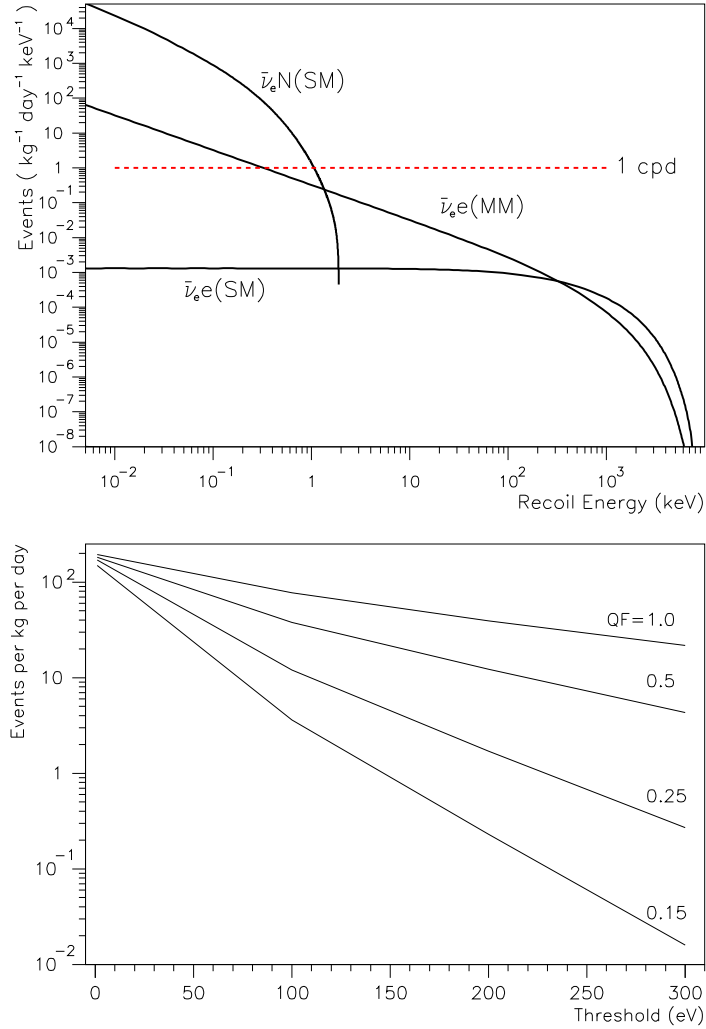


Fig. 1. (a) Top: The differential cross-section of the various neutrino interaction channels, at KS-Lab with Ge as the target isotope. The background level of 1 cpd is also shown. (b) Bottom: The variations of the neutrino coherent scattering event rates versus threshold at different quenching factors for a 1 kg ULEGe detector at KS-Lab.

known particle neutrino is an important milestone as well. Furthermore, neutrino coherent scattering may be a promising avenue towards a compact and relatively transportable neutrino detector, an application of which can be for the real-time monitoring on the operation of nuclear reactors^{16,17}, a subject of paramount global importance in the non-proliferation of nuclear materials.

Nuclear power reactors are intense source of electron anti-neutrinos ($\bar{\nu}_e$) at the MeV range, from which many important neutrino experiments were based. The $\bar{\nu}_e$ -

4 *Henry T. Wong*

spectra are well-modeled, while good experimental control is possible via the reactor ON/OFF comparisons. The magnetic moment results at KS² set the stage to pursue the studies of neutrino-nucleus coherent scatterings with reactor neutrinos⁷.

The maximum nuclear recoil energy at momentum transfer much larger than neutrino masses is given by:

$$T_N^{\max} = \frac{2E_\nu^2}{M_N + 2E_\nu} \quad (3)$$

The maximum neutrino energy for the typical reactor $\bar{\nu}_e$ spectra is about 8 MeV, such that $T_N^{\max} = 1.9$ keV for Ge target ($A=72.6$). The differential cross section for coherent scattering versus nuclear recoil energy with typical reactor $\bar{\nu}_e$ spectra is displayed in Figure 1a. Overlaid for comparisons are the contributions due to neutrino-electron scatterings from the Standard Model and magnetic moment effects at the present limit, as well as the 1 cpd benchmark background level.

In ionization detectors like HPGe, the measure-able energy is only a fraction of the energy deposit for the nuclear recoil events which have large dE/dx . The *quenching factor* (QF), defined as the ratio of the measure-able to the deposit energy, is about 0.2-0.25 for Ge in the <10 keV region¹⁸. Accordingly, the maximum measure-able energy for nuclear recoil events in Ge due to reactor $\bar{\nu}_e$ is about 400-500 eV.

The event rates for neutrino-nucleus coherent scattering at different threshold and quenching factors at KS are depicted in Figure 1b. The goals of the R&D program is to devise an experiment based on Ge-detector with a mass range of 1 kg, a threshold as low as 100 eV, and an on-site background level of 1 cpd below 1 keV. At the typical $QF=0.25$, the event rate for such configurations will be $11 \text{ kg}^{-1} \text{ day}^{-1}$ or $4000 \text{ kg}^{-1} \text{ yr}^{-1}$, at a signal-to-background ratio of >22 .

2.2. Neutrino Magnetic Moments

Neutrino magnetic moments (μ_ν) are parameters characterizing the spin-dependent couplings of the neutrinos to the photons⁸. A limit of

$$\mu_{\bar{\nu}_e} < 7.4 \times 10^{-11} \mu_B \quad (4)$$

at 90% confidence level (CL) has been achieved at KS-Lab with a high-purity germanium detector at a threshold of 12 keV and a background level of 1 cpd². This result was further improved upon by the GEMMA experiment¹⁹ with a similar design but at a closer location to the reactor core.

A natural by-product of a detector with kg-mass, 100 eV threshold and 1 cpd background level would be to further enhance the sensitivities of μ_ν -searches at reactors. The physics threshold can be as low as 500 eV just above the coherence scattering detectable energy cut-off. A finite μ_ν will contribute to ν -e scattering with a differential cross-section term given by:

$$\left(\frac{d\sigma}{dT}\right)_{\mu_\nu} = \frac{\pi\alpha_{\text{em}}^2\mu_\nu^2}{m_e^2} \left[\frac{1-T/E_\nu}{T}\right]. \quad (5)$$

The effects are much enhanced at this sub-keV energy due to the $1/T$ dependence, as illustrated in Figure 1a. An improved sensitivity range down to $\sim 10^{-11} \mu_B$ can be expected.

2.3. Cold Dark Matter Searches

There are compelling evidence that about 25% of the energy density in the universe is composed of Cold Dark Matter^{9,15} due to a not-yet-identified particle, generically categorized as Weakly Interacting Massive Particle (WIMP, denoted by χ). A direct experimental detection of WIMP is one of the biggest challenges in frontier astroparticle physics.

The WIMP will interact with matter pre-dominantly via the same coherent scattering mechanism like the neutrinos:

$$\chi + N \rightarrow \chi + N . \quad (6)$$

The major difference is that cosmology dictates that the WIMPs should be massive and its motion non-relativistic to be consistent with the observational data on structure formation⁹. In addition, it is possible to have a spin-dependent interaction between WIMP and matter.

Supersymmetric (SUSY) particles⁹ are the leading WIMP candidates. The popular SUSY models prefer WIMP mass (m_χ) of the range of ~ 100 GeV, though light neutralinos remain a possibility²⁰. Most experimental programs optimize their design in the high-mass region and exhibit diminishing sensitivities for $m_\chi < 10$ GeV, where there is an allowed region if the annual modulation data of the DAMA experiment²¹ are interpreted as WIMP signatures. Simple extensions of the Standard Model with a singlet scalar favors light WIMPs²². To probe the low-mass region, detector with sub-keV threshold is necessary. Such threshold will also allow the studies of WIMPs bound in the solar system²³, and non-pointlike SUSY candidates like Q-balls²⁴, but presents a formidable challenge to detector technology and to background control.

In direct WIMP search experiments, the observed nuclear recoil rate per unit detector mass (dR/dT_N) at recoil energy T_N is related to the elastic WIMP-nucleon cross section ($\sigma_{\chi N}$) and m_χ via²⁵:

$$\frac{dR}{dT_N} = \left[\frac{\rho_\chi}{2 m_\chi \mu_N^2} \right] \left[\left(\frac{\mu_A^2}{\mu_N^2} \right) \left(\frac{C_A}{C_N} \right) F^2(q) \sigma_{\chi N} \right] \int_{v_{min}} \frac{f(\vec{u}, t)}{u} d^3u , \quad (7)$$

where $\mu_{A/N}$ denotes the reduced mass of the target nucleus/nucleon with respect to the WIMPs, while $F(q)$ is the nuclear form factor where $q = \sqrt{(2M_A T_N)}$ is the nucleus recoil momentum, $\rho_\chi \sim 0.3 \text{ GeVcm}^{-3}$ is the standard local (solar neighborhood) halo WIMP density, $f(\vec{u}, t)$ is the time-dependent distribution of the WIMP velocity \vec{u} relative to the detector typically assumed to be Maxwellian with a cut-off at the galactic escape velocity. The lower bound of the integral

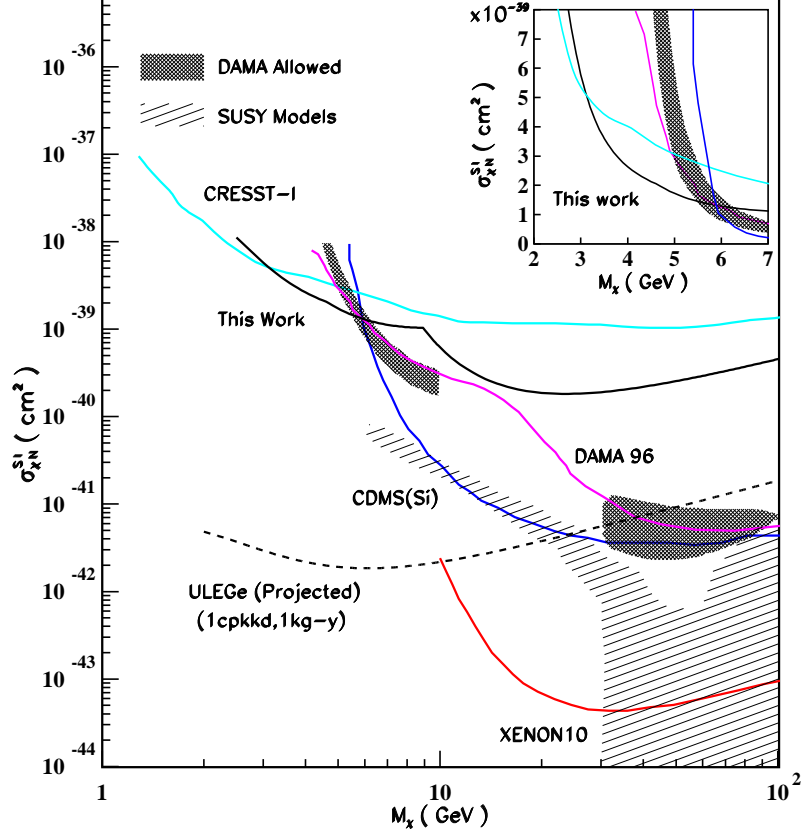
6 *Henry T. Wong*

Fig. 2. Exclusion plots of spin-independent χN cross-section versus WIMP-mass, displaying the KS-ULEGe limits and those from various experiments defining the current boundaries. The DAMA allowed regions are superimposed. The striped region is that favored by SUSY models. Projected sensitivities of full-scale experiments are indicated as dotted lines. The relevant region is presented with linear scales in the inset.

$v_{min} = \sqrt{(M_A T_N)/(2\mu_\chi^2)}$ denotes the minimal WIMP velocity necessary to kinematically induce a nuclear recoil interaction. The enhancement factor from nucleon to nucleus is denoted by (C_A/C_N) , which is equal to A^2 due to coherent effects for spin-independent couplings. In the spin-dependent case²⁶, couplings of the WIMPs to protons and neutrons are in general different, depending on

$$C_A = \left(\frac{8}{\pi}\right) [a_p \langle S_p \rangle + a_n \langle S_n \rangle]^2 \left(\frac{J+1}{J}\right) ; \quad C_{p/n} = \left(\frac{6}{\pi}\right) a_{p/n}^2 \quad (8)$$

where J is total nuclear spin, $a_{p/n}$ are the WIMP-proton/neutron coupling constants and $\langle S_{p/n} \rangle$ are the expectation values of the proton/neutron spins within the nucleus²⁷. At the typical range of $m_\chi \sim 10$ GeV, the maximal WIMP velocity of $v \sim 0.002c$ corresponds to a kinetic energy of $T_\chi \sim 20$ keV and the maximal recoil energy at Ge of $T_N \sim 5$ keV.

The uniqueness and advantages of having a low-threshold detector are twofold. Firstly, WIMPs with lower masses become detectable at a lower threshold, as indicated in Eq. 7, thereby opening a new window of observation. Secondly, the lower bound of the integral v_{\min} in Eq. 7, which represents the minimum velocity of a WIMP that produces a recoil energy T_N , is proportional to T_N . Therefore, a lower threshold allows a larger range of WIMPs to contribute in an observable interaction and hence results in better sensitivities for all values of m_χ .

A summary of the sensitivities of the spin-independent cross-section ($\sigma_{\chi N}^{\text{SI}}$) versus m_χ is depicted in Figure 2. The best sensitivities to date in the low WIMP mass region ($m_\chi < 10$ GeV) are due to data taken at KS with a ultra-low-energy germanium prototype⁶ with threshold of 200 eV, superseding those from the previous CRESST-I experiment²⁸ with sapphire(Al_2O_3)-based cryogenic detector at a threshold of 600 eV. The other experiments defining the current boundaries²⁹ as well as the DAMA-allowed regions²¹ are superimposed. The striped region is that favored by SUSY models²⁰. Projected sensitivities of full-scale experiments are indicated as dotted lines.

3. Ultra-Low-Energy Germanium Detector

Although the νN and χN cross-section of Eq. 2 is relatively large due to the respective N^2 and A^2 enhancement by coherence, the small kinetic energy from nuclear recoils poses severe experimental challenges both to the detector sensitivity and to background control. Various detection schemes using cryogenic³⁰, gas^{14,31} or liquid-gas two phase¹⁷ detectors have been investigated taking reactor neutrinos as the source. There was a recent study on using neutrino beam from stopped-pion facilities¹². Alternatively, germanium-based ionization detectors^{7,32} offer a more matured technology, less costly to build and to operate, more compact, and easier to scale-up. This detector technology has been widely and successfully used in various areas of low energy neutrino physics and cold dark matter searches.

“Ultra-Low-Energy” Germanium (ULEGe) detectors, developed originally for soft X-rays detection, are candidate technologies to meet these challenges of probing into the previously unexplored low-energy domain. These detectors typically have modular mass of 5-10 grams while detector array of up to $N=30$ elements have been successfully built. Various ULEGe prototypes³³ were constructed in the course of our R&D program, the highlights of which are discussed in the following sections. Complementary to these, measurements of QF in Ge at the sub-keV range is pursued at a neutron facility, following the previous successful measurements of QF in CsI(Tl)³⁴.

3.1. Detector Threshold

A typical measured energy spectrum ULEGe prototype is depicted in Figure 3a. Pulsed optical feedback preamplifiers were used to extract the signals from the electron-hole pairs. The output was transferred to two amplifiers at 6 μs and 12 μs

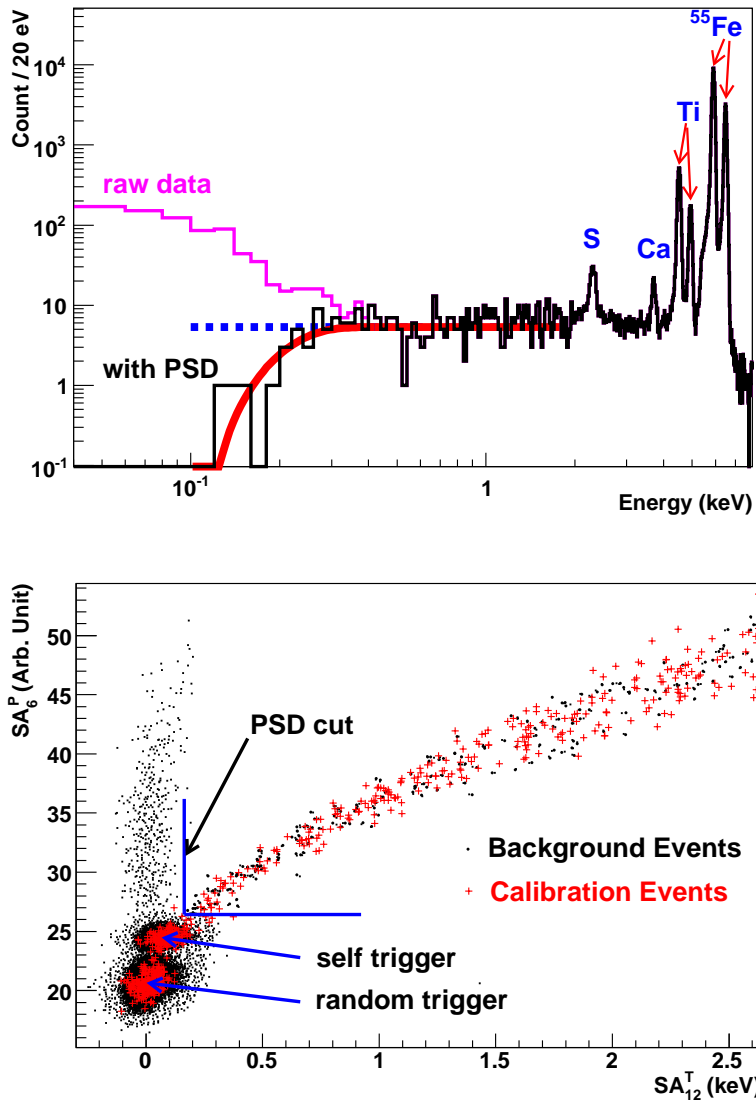


Fig. 3. (a) Top: Measured energy spectrum of the ULEGe with ^{55}Fe source showing also X-ray peaks from various materials. The best-fit of the spectrum at 0.5 – 2 keV is extrapolated to low energy. The black histogram represents events selected by PSD cuts. Deviations from the expected spectra contribute to PSD efficiencies. (b) Bottom: Scattered plots of the two signals with different shaping times and amplification factors, which are constrained by both energy and timing, for both calibration and physics events. The PSD selection is shown.

shaping time, and read out by a 20 MHz Flash Analogue Digital Converter³⁵. The sampling period extended from $t=-20\ \mu$ to $70\ \mu\text{s}$ where $t=0$ was defined by the trigger instant. Calibration was achieved by external ^{55}Fe X-ray sources (5.90

and 6.49 keV) together with X-rays from titanium (4.51 and 4.93 keV), calcium (3.69 keV) and sulphur (2.31 keV). Excellent linearity down to threshold was demonstrated with a test-pulsar. A random trigger uncorrelated to the detector provided the dead time and efficiencies measurements as well as the zero-energy calibration. The electronic noise which defines the threshold can be suppressed by pulse shape discrimination (PSD) through correlating the two output signals at the two shaping times, as illustrated in Figure 3b. A threshold of 200 eV at $\sim 50\%$ selection efficiency⁶ was achieved.

3.2. Background Measurement

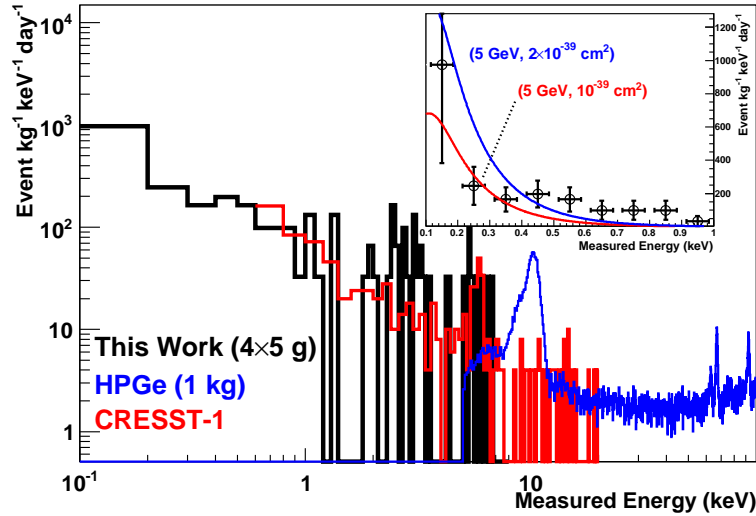


Fig. 4. The measured spectrum of ULEGe with 0.338 kg-day of data, after cosmic-ray and anti-Compton vetos as well as PSD selections. Background spectra of the CRESST-I experiment and the HPGe are overlaid for comparison. The expected nuclear recoil spectra for two cases of $(m_\chi, \sigma_{\chi N}^{\text{SI}})$ are superimposed onto the spectrum shown in linear scales in the inset.

Background studies were made with the prototypes at the KS reactor laboratory and at the Yangyang Underground laboratory (Y2L) in South Korea. The detectors were surrounded by active anti-Compton crystal scintillator detectors, passive shieldings as well as active cosmic-ray veto scintillators – identical to the those for the KS 1 kg HPGe experiment². Data were taken under different hardware and software configurations. The best spectrum in terms of background and threshold is shown in Figure 4, with those from CRESST-1²⁸ and the 1-kg HPGe² superimposed. The background was translated to the WIMP exclusion regions⁶ in Figure 2 via Eq. 7. The KS ULEGe data define the exclusion boundary for $m_\chi \sim 3 - 6$ GeV. Further work on background understanding and suppression are under way.

3.3. Detector Mass Scale-Up

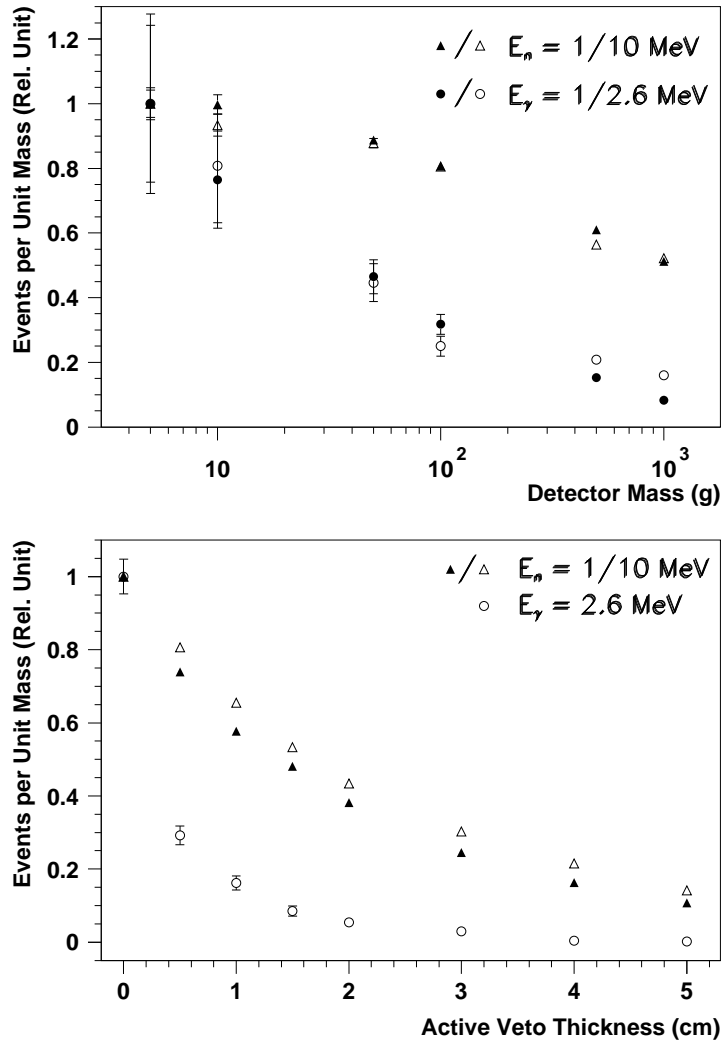


Fig. 5. (a) Top: Simulated background rates at the sub-keV range per unit mass versus detector mass at the same external γ -background level. (b) Bottom: Background reduction factors in a 1-kg detector versus thickness of 4π Ge-veto layer. Photon energy of 1.0 and 2.6 MeV and neutron energy of 1.0 and 10 MeV were adopted.

The ULEGe element can be constructed in multi-array configuration. Alternatively, “segmented” ULEGe detector read out as pixels in integrated sensors have been constructed and is being studied. Moreover, inspired by a novel design in the 1980’s³⁶, there are recent important advances in the construction of a single-element

ULEGe of 500-g mass³², with which a detector threshold of 300 eV was demonstrated. This offers great potentials of scaling-up the detector mass to the kg-range and beyond with simple electronics and data acquisition schemes.

Realistic simulations were performed on the behaviour of photons and neutrons with kg-scale ULEGe. The variations of the “after-cut” rates with detector mass are depicted in Figure 5a. The mass-normalized count rates at low energy (<10 keV) under a constant external γ -background decrease by a factor of 10 for increasing Ge target mass from 5 g to 1 kg, due to self-absorption of the target. Similar behaviour applies to neutron-induced background, though the difference is less. Illustrated in Figure 5b are the background reduction factors for a 1 kg detector versus the thickness of possible Ge-veto layers. The potential reach on $\sigma_{\chi N}^{\text{SI}}$ sensitivities with a 1-kg detector at 1 cpd background is depicted in Figure 2.

4. Outlook

A detector with 1 kg mass, 100 eV threshold and 1 cpd background level has important applications in neutrino and dark matter physics, as well as in the monitoring of reactor operation. Crucial advances have been made in adapting the ULEGe technology to meet these challenges. Competitive limits have been achieved in prototype studies on the WIMP dark matter spin independent couplings. Intensive research programs are being pursued along these fronts towards realization of such experiments.

Acknowledgments

The author is grateful to the CosPA-2007 Symposium for the opportunity to present this report. This work is supported by contracts NSC94-2112-M-001-028 and NSC 96-2112-M-001-005 from the National Science Council, Taiwan, as well as by the Pilot Project Scheme 2004-06 from the Academia Sinica, Taiwan. The Y2L-related work is supported by funding support from the National Natural Science Foundation, China through contract 10620140100. The QF measurement is supported by neutron facility at the China Institute of Atomic Energy. The infrastructure support at Y2L is provided by KIMS Collaboration, South Korea.

References

1. H.T. Wong, *Mod. Phys. Lett. A* **19**, 1207 (2004).
2. H.B. Li et al., *Phys. Rev. Lett.* **90**, 131802 (2003); H.T. Wong et al., *Phys. Rev. D* **75**, 012001 (2007).
3. B. Xin et al., *Phys. Rev. D* **72**, 012006 (2005).
4. H.M. Chang et al., *Phys. Rev. D* **75**, 052004 (2007).
5. H.B. Li et al., *Nucl. Instrum. Methods A* **459**, 93 (2001); Y. Liu et al., *Nucl. Instrum. Methods A* **482**, 125 (2002).
6. S.T. Lin et al., arXiv: hep-ex/0712.1645 (2007).
7. H.T. Wong et al., *J. Phys. Conf. Ser.* **39**, 266 (2006).

12 *Henry T. Wong*

8. H.T. Wong and H.B. Li, *Mod. Phys. Lett.* **A 20**, 1103 (2005); H.T. Wong, *Nucl. Phys. B (Proc. Suppl.)* **143**, 205 (2005).
9. See the respective sections in *Review of Particle Physics*, W.M. Yao et al., *J. Phys.* **G 33** (2006), for details and references.
10. D.S. Freedman, *Phys. Rev.* **D 9**, 1389 (1974); Y.V. Gaponov and V.N. Tikhonov, *Sov. J. Nucl. Phys.* **26**, 31 (1977); L.H. Sehgal and M. Wanninger, *Phys. Lett.* **B 171**, 107 (1986).
11. L.M. Krauss, *Phys. Lett.* **B 269**, 407 (1991); J. Barranco, O.G. Miranda and T.I. Rashba, *J. High Energy P.* **12**, 021 (2005); J. Papavassiliou, J. Bernabéu and M. Passera, *Proc. of Science (HEP2005)*, 192 (2006); J. Barranco, O. G. Miranda and T. I. Rashba, *Phys. Rev.* **D 76**, 073008 (2007).
12. K. Scholberg, *Phys. Rev.* **D 73**, 033005 (2006).
13. J.R. Wilson, *Phys. Rev. Lett.* **32**, 849 (1974); D.Z. Freedman, D.N. Schramm and D.L. Tubbs, *Annu. Rev. Nucl. Sci.* **27**, 167 (1977).
14. S. Rune et al., *AIP Conf. Proc.* **785** 110 (2005).
15. R.J. Gaijskell, *Annu. Rev. Nucl. Part. Sci.*, **54**, 315 (2004), and references therein.
16. J. Learned, *Nucl. Phys. B (Proc. Suppl.)* **143**, 152 (2005).
17. C. Hagmann and A. Bernstein, *IEEE Tran. Nucl. Sci.* **51**, 2151(2004).
18. K.W. Jones and H.W. Kraner, *Phys. Rev.* **C 1**, 125 (1971); K.W. Jones and H.W. Kraner, *Phys. Rev.* **A 11**, 1347 (1975); T. Shutt et al., *Phys. Rev. Lett.* **24**, 3425 (1992); Y. Messous et al., *Astropart. Phys.* **3**, 361 (1995).
19. A.G. Beda et al., arXiv:hep-ex/0705.4576 (2007).
20. A. Bottino et al., *Phys. Rev.* **D 72**, 083521 (2005).
21. C. Savage, P. Gondolo and K. Freese, *Phys. Rev.* **D 70**, 123513 (2004); P. Gondolo and G. Gelmini, *Phys. Rev.* **D 71**, 123520 (2005).
22. X.G. He et al., *Mod. Phys. Lett.* **A 22**, 2121 (2007).
23. T. Damour and L.M. Krauss, *Phys. Rev. Lett.* **81**, 5726 (1998); J.I. Collar, *Phys. Rev.* **D 59**, 063514 (1999).
24. G. Fleming, A. Kusenko and S. Nussinov, *Phys. Rev. Lett.* **89**, 101302 (2002).
25. J.D. Lewin and P.F. Smith, *Astropart. Phys.* **6** 87 (1996).
26. D.R. Tovey et al., *Phys. Lett.* **B 488**, 17 (2000).
27. V.I. Dimitrov, J. Engel and S. Pittel, *Phys. Rev.* **D 51**, 291 (1995).
28. G. Angloher et al., *Astropart. Phys.* **18**, 43 (2002).
29. R. Bernabei et al., *Phys. Lett.* **B 389**, 757 (1996); D.S. Akerib et al., *Phys. Rev. Lett.* **96**, 011302 (2006); J. Angle et al., *Phys. Rev. Lett.* **100**, 021303 (2008).
30. A. Drukier and L. Stodolsky, *Phys. Rev.* **D 30**, 2295 (1984); B. Cambrea, L.M. Krauss, and F. Wilczek, *Phys. Rev. Lett.* **55**, 25 (1985); L. Oberauer, *Prog. Part. Nucl. Phys.* **48**, 301 (2002).
31. P. Barbeau et al., *IEEE Tran. Nucl. Sci.* **50**, 1285 (2003).
32. P.A. Barbeau, J.I. Collar, and O. Tench, *JCAP* **09**, 009 (2007).
33. Manufacturer: Canberra Industries, Inc.
34. M.Z. Wang et al., *Phys. Lett.* **B 536**, 203 (2002).
35. W.P. Lai et al., *Nucl. Instrum. Methods* **A 465**, 550 (2001).
36. P.M. Luke et al., *IEEE Trans. Nucl. Sci.* **36**, 926 (1989).